Modeling the current-voltage characteristics of bilayer polymer photovoltaic devices

J. A. Barker, C. M. Ramsdale, and N. C. Greenham
Cavendish Laboratory, Madingley Road, Cambridge CB3 0HE, United Kingdom
(Received 22 August 2002; published 18 February 2003)

We have developed a numerical model to predict the current-voltage curves of bilayer conjugated polymer photovoltaic devices. The model accounts for charge photogeneration, injection, drift, diffusion, and recombination, and includes the effect of space charge on the electric field within the device. Charge separation at the polymer-polymer interface leads to the formation of bound polaron pairs which may either recombine monomolecularly or be dissociated into free charges, and we develop expressions for the field dependence of the dissociation rate. We find that the short-circuit quantum efficiency is determined by the competition between polaron pair dissociation and recombination. The model shows a logarithmic dependence of the open-circuit voltage on the incident intensity, as seen experimentally. This additional intensity-dependent voltage arises from the field required to produce a drift current that balances the current due to diffusion of carriers away from the interface.

DOI: 10.1103/PhysRevB.67.075205 PACS number(s): 72.20.Ee, 72.20.Jv, 72.80.Le

I. INTRODUCTION

Polymer photovoltaic devices are a potentially attractive alternative to silicon solar cells, due to their low cost, ease of fabrication, and process temperatures which are suitable for fabrication onto lightweight plastic substrates.[1] Power conversion efficiencies for polymer devices are not yet high enough for these to be commercially viable, but devices based on polymer blends and bilayers show significant improvements in conversion efficiency over single-component devices, as a result of enhanced charge separation at the polymer-polymer interface.[2–4] In order to optimize the power conversion efficiency of these devices, it is important to understand the distributions of charge density and electric field in the devices under various operating conditions, and to quantify the loss mechanisms which are expected to occur. Due to the very different generation, transport and recombination processes which occur in organic semiconductors, simple models developed for inorganic photovoltaic devices do not necessarily apply. Photoconductivity in intrinsic semiconductors has been extensively studied[5] and various authors have discussed the origin of the open-circuit voltage in blends of C_{60} with conjugated polymers,[6,7] however, modeling specific to polymer photovoltaic devices has concentrated on single-layer devices, where carrier generation occurs at the electrodes.[8] It is therefore necessary to develop new models for organic devices, where charge carrier photogeneration occurs at the interface between two thin, undoped, low-mobility semiconductors.

In this paper, we develop a numerical model for the generation, transport and recombination of charges in a bilayer photovoltaic device. We are able to model current-voltage characteristics for the device under illumination, taking into account space charge and the effects of dissociation and recombination of polaron pairs at the polymer-polymer interface. We investigate the factors that influence the open-circuit voltage in these devices, which has been found experimentally to be larger than the difference in the electrode work functions.[9] The results of the model are in good agreement with experimental measurements on bilayer polyfluorene devices, and show that the additional contribution to the open-circuit voltage V_{oc} is largely due to the diffusion of carriers away from the interface.

II. EXPERIMENTAL DATA

Bilayer devices were fabricated by a lamination technique using poly(9,9′-dioctylfluorene-co-benzothiadiazole) (F8BT) and poly(9,9′-dioctylfluorene-co-bis-N, N′-(4-butylphenyl)-bis-N,N′-phenyl-1,4-phenylenediamine) (PFB) as electron- and hole-transporting layers respectively. The anode was indium-tin oxide and a range of metals with different work functions were used as cathodes. The fabrication and characterization of these devices has been reported previously;[9] here we reproduce for convenience the results which are of particular interest for modeling. A schematic energy-level structure of the device is shown in Fig. 1. Figure 1(b) shows the device under flat-band conditions, corresponding to an applied voltage equal to the difference in electrode work functions. At short circuit [Fig. 1(a)], the electrode Fermi levels are aligned, corresponding to an inter-

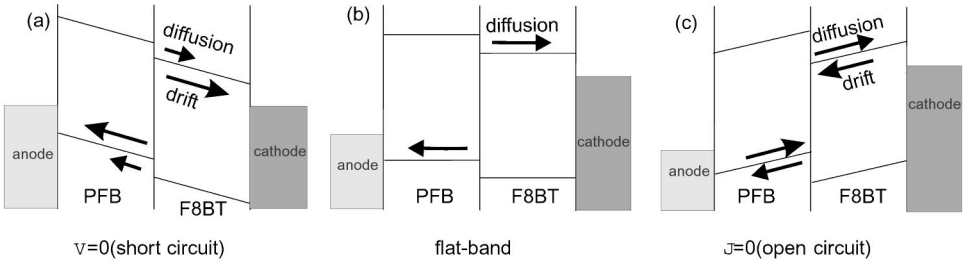

FIG. 1. Schematic band diagrams for an anode/PFB/F8BT/cathode device under (a) short-circuit, (b) flat-band, and (c) open-circuit conditions. Arrows indicate the flux of carriers under illumination, due to drift and diffusion.

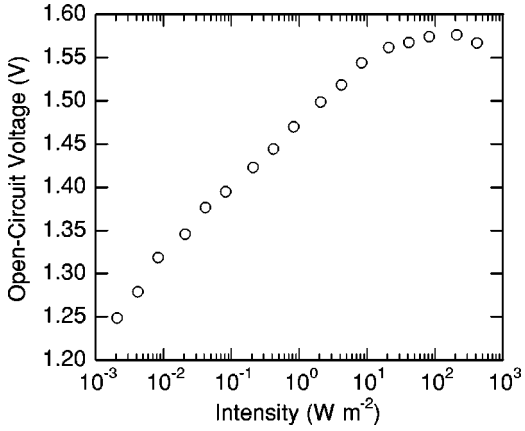

FIG. 2. Measured open-circuit voltage for an ITO/PFB[50 nm]/F8BT[100 nm]/Al device as a function of incident intensity at 458 nm.

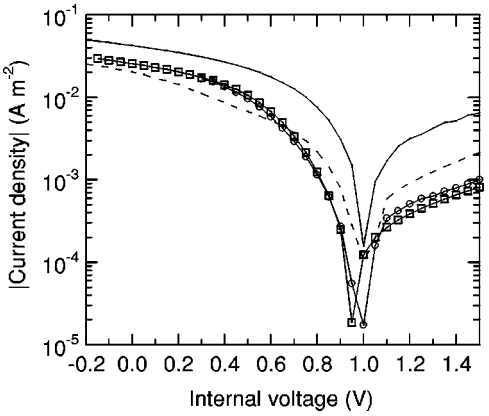

FIG. 3. Measured current density versus internal voltage for ITO/PFB[50nm]/F8BT[100nm]/cathode devices, under illumination at 459 nm with an intensity of 7 W m^{-2}. The cathodes are gold (circles), copper (squares), chromium (solid line), and aluminum (dotted line).

nal field that will sweep electrons generated at the interface towards the cathode, and holes towards the anode. At the open-circuit voltage [Fig. 1(c)], the total current is zero. Under illumination, photogenerated carriers are generated at the interface, leading to a diffusion current away from the interface which must be balanced by a drift current to achieve zero net current. The drift current requires an internal electric field, provided by the additional voltage beyond the flat-band condition. A simple analytical model for this extra open-circuit voltage[9] considers a voltage V_1 dropped linearly across the electron-transporting layer of the device, thickness L. The sum of drift and diffusion currents is zero when the electron density n varies with distance from the interface, z, as

$$n(z)=n(0)\exp\left(-\frac{eV_1}{k_BT}\frac{z}{L}\right). \tag{1}$$

If we assume that the electron density at the interface, n_{int}, is related to the incident intensity by a power law,

$$n_{int}=k_1 I^{\alpha}, \tag{2}$$

then we find that

$$\frac{eV_1}{k_BT}\simeq \alpha \ln I+\ln k_1-\ln n_{cath}, \tag{3}$$

where n_{cath} is the electron density at the cathode.

Performing a similar calculation for the hole-transporting side of the device, assuming $p_{int}=k_2 I^{\alpha}$, gives the total open-circuit voltage

$$\frac{eV_{oc}}{k_BT}\simeq 2\alpha \ln I+\ln k_1+\ln k_2-\ln n_{cath}-\ln p_{an}, \tag{4}$$

where p_{an} is the hole density at the anode.

The variation of the measured open-circuit voltage with intensity for a device with an aluminum cathode is shown in Fig. 2. Over the same range of intensities, the short-circuit current is found to be linearly dependent on intensity in this device.[9] The simple model gives a reasonable fit to the measured variation of V_{oc} with intensity before saturation occurs, assuming that $\alpha=0.5$ and that the carrier densities at the electrodes are insensitive to intensity. Numerical modeling will allow α, n_{cath}, and p_{an} to be determined self-consistently to check the validity of the simple model, and will also allow the effects of space charge to be included.

Numerical modeling will also enable the full current-voltage characteristics under illumination to be predicted. The experimental characteristics for various cathodes are shown in Fig. 3. For the purpose of modeling we are concerned only with the internal field, so it is convenient to define our voltage relative to the flat-band voltage, by subtracting the difference in electrode work functions from the true applied voltage. All current-voltage characteristics in this paper are plotted with respect to this ''internal'' voltage. In Fig. 3 the internal voltage has been calculated using literature values for the cathode work functions, and assuming an ITO work function of 4.8 eV.[9] If the open-circuit voltage were simply due to the difference in work functions of the electrodes, then Fig. 3 would show the zero current at zero voltage. In fact there is an extra contribution to V_{oc} of ≈ 1 V in all these devices under illumination at 7 W m^{-2}.

III. THEORY

The steady-state charge distributions within each layer are found from the self-consistent numerical solution of the Poisson equation and the continuity equations. This gives the electron and hole number densities, n and p, as

$$\frac{\partial n}{\partial t}=\frac{\partial}{\partial z}\left[-\mu_n k_B T\frac{\partial n}{\partial z}-\mu_n neE\right]-R_{np}, \tag{5}$$

$$\frac{\partial p}{\partial t}=\frac{\partial}{\partial z}\left[-\mu_p k_B T\frac{\partial p}{\partial z}+\mu_p peE\right]-R_{np}, \tag{6}$$

$$\mu_{n(p)}=\mu_{n0(p0)}\exp[\gamma\sqrt{E}], \tag{7}$$

$$\frac{\partial E}{\partial z}=\frac{e(p-n)}{\varepsilon_0\varepsilon_r}, \tag{8}$$

where $\partial n/\partial t$ and $\partial p/\partial t$ are zero at steady state. μ_{n0} and μ_{p0} are the zero-field carrier mobilities, γ describes the field dependence of the mobility, E is the electric field strength, and ε_r is the relative permitivity of the material, which typically takes a value of 4 for polymer systems. These equations have previously been successfully used to model the properties of polymer light-emitting diodes (LEDs).[10–13] In the equations above, the diffusion coefficient is taken to be related to the mobility by the Einstein relationship, although we note that at high carrier densities the diffusion coefficient may be increased.[14] When the applied bias is sufficiently below V_{oc}, the electric field will be in such a direction as to sweep electrons towards the cathode and holes towards the anode. Under these conditions we assume rapid extraction of charge carriers at the electrodes. As we saw in Fig. 1, under some conditions the field at the electrodes is reversed, such that carriers are injected from the electrodes. Due to the effects of disorder, it is difficult to obtain an accurate analytical expression for charge injection into a polymer. Here, we use the thermionic emission model of Scott and Malliaras,[15] assuming a site density of 10^{27} m^{-3}. For most of our modeling we assume injection barriers of 0.5 eV at both the anode and cathode, and we then go on to study the effect of variation of these barriers. The recombination rate R_{np} will follow a Langevin-like rate, but we find that this process is negligible since each layer contains predominantly only one carrier type.

To extend these equations to treat photovoltaic devices it is necessary to model the generation and recombination of charge at the polymer-polymer interface. Light absorbed in the device will produce excitons, some of which may diffuse to the interface where rapid charge transfer will occur. In principle, it is possible to model the fraction of incident light that will lead to charge separation,[16,17] however, since the exciton diffusion lengths in our polymers are not well known, we will use the exciton dissociation rate per unit area, G_X, rather than the incident light intensity as the input parameter in our model. For reference, if we assume an exciton diffusion length of 5 nm in F8BT, an incident power of 1 W m^{-2} at 459 nm corresponds to an exciton dissociation rate of order 2×10^{17} m^{-2} s^{-1}. In the simplest possible model, exciton dissociation at the interface would produce free charges which would then either be extracted from the device or recombine in a bimolecular fashion at the interface. Experimentally, the short-circuit photocurrent is found to depend linearly on the incident light intensity, however, under these conditions recombination clearly limits the quantum efficiency since higher quantum efficiencies can be achieved at more negative biases. This is inconsistent with a bimolecular recombination mechanism, which would lead to a sublinear intensity dependence. This issue can be resolved by realizing that the initial exciton dissociation event in fact produces a pair of charges which are still coulombically bound (a polaron pair). These polaron pairs can then either recombine monomolecularly (with a rate constant k_{rec} corresponding to a lifetime τ_{rec}), or may be dissociated into free carriers with a field-dependent rate constant $k_{diss}(E)$. Also, polaron pairs may be formed by bimolecular capture of free charges at the interface, with a rate F_X. The areal density of polaron pairs at the interface X therefore follows the rate equation

$$\frac{\partial X}{\partial t} = G_X - k_{rec}X - k_{diss}(E)X + F_X . \tag{9}$$

We assume that dissociation of polaron pairs produces free carriers in the first layer of polymer chains either side of the interface. We define the separation between polymer chains in the electric field direction to be h, which we take to have a value of 1 nm. Within a distance h of the interface, the continuity equations for electrons and holes in the electron- and hole-transporting polymers respectively are modified as follows:

$$\frac{\partial n}{\partial t} = \frac{\partial}{\partial z}\left[-\mu_n \frac{k_B T}{e}\frac{\partial n}{\partial z} - \mu_n n E \right] + \frac{k_{diss}(E)X - F_X}{h}, \tag{10}$$

$$\frac{\partial p}{\partial t} = \frac{\partial}{\partial z}\left[-\mu_p \frac{k_B T}{e}\frac{\partial p}{\partial z} + \mu_p p E \right] + \frac{k_{diss}(E)X - F_X}{h}. \tag{11}$$

We neglect hopping of electrons and holes over the barrier at the interface, on the basis that this is likely to result in rapid formation of excitons close to the interface, which will subsequently be dissociated back across the interface. This approximation is consistent with the low electroluminescence efficiencies seen in these devices at positive biases. We also include the effect of the polaron pairs on the electric field at the interface, assuming that the charges in a polaron pair are localized within a distance h of the interface. The polaron pairs contribute an additional change in electric field across the polymer chains adjacent to the interface, given by

$$\Delta E_e = -\frac{eX}{\varepsilon_0 \varepsilon_r}, \tag{12}$$

$$\Delta E_h = \frac{eX}{\varepsilon_0 \varepsilon_r}, \tag{13}$$

where ΔE_e and ΔE_h represent the additional change in field across a distance h in the electron- and hole-accepting polymers, respectively. The polaron pairs thus produce a dipole which causes an additional change in potential in the region of the interface.

Next we require an expression for the rate of polaron pair dissociation into free charges, $k_{diss}(E)$. A full treatment including the effects of disorder is beyond the scope of this work, since it requires detailed Monte Carlo simulations.[18] In order to obtain a physically reasonable approximation for the field dependence of the dissociation rate, we follow a simple approach which neglects disorder. We note that the electron and hole which make up the polaron pair are each only able to escape their mutual coulomb potential over a half surface. The zero-field dissociation rate constant $k_{diss}(0)$ is then

$$k_{diss}(0) = \int_0^{2\pi} d\psi \int_0^{\pi/2} sin(\theta) d\theta A \exp\left[-\frac{U_B}{k_B T} \right], \tag{14}$$

where U_B is the polaron pair binding energy and A is a constant related to the attempt frequency for escape. We define the zero-field dissociation time $\tau_{diss}=k_{diss}^{-1}(0)$. Poole-Frenkel-like enhancement of the dissociation rate will occur at negative applied field, where the barrier to carrier escape is lowered by some energy, $U_M(\theta)$, whose value depends on the angle θ between the direction of escape and the applied field direction. Following the treatment of Jonscher,[19] the separation r_M required to reach the top of the barrier is given by

$$r_M=\sqrt{\frac{-e}{4\pi\varepsilon_0\varepsilon_r E\cos(\theta)}}. \tag{15}$$

It then follows that

$$U_M(\theta)=\sqrt{\cos(\theta)}\sqrt{\frac{-e^3E}{\pi\varepsilon_0\varepsilon_r}}. \tag{16}$$

Using this result in the integral for $k_{diss}(E)$ with $E<0$ gives

$$k_{diss}(E)=\frac{k_{diss}(0)}{M}\left[\exp[M]\left(1-\frac{1}{M}\right)+\frac{1}{M}\right], \tag{17}$$

$$M=\frac{e}{k_BT}\sqrt{\frac{-eE}{\pi\varepsilon_0\varepsilon_r}}. \tag{18}$$

At positive applied fields, exciton dissociation will be suppressed, however, it is more difficult to define the point of charge separation since there is no maximum in the potential for separation against the applied field. We, therefore, define the point of charge separation as where the coulombic binding energy of the polaron pair is equal to k_BT, which occurs at the capture radius

$$r_c=\frac{e^2}{4\pi\varepsilon_0\varepsilon_r k_BT}. \tag{19}$$

Compared with the zero-field case, this requires an extra energy

$$U_E=\frac{e^3E\cos\theta}{4\pi\varepsilon_0\varepsilon_r k_BT}. \tag{20}$$

Integrating as before with $E>0$ gives

$$k_{diss}(E)=k_{diss}(0)\frac{4\pi\varepsilon_0\varepsilon_r k_B^2T^2}{e^3E}\left(1-\exp\frac{-e^3E}{4\pi\varepsilon_0\varepsilon_r k_B^2T^2}\right). \tag{21}$$

Next we consider the formation of polaron pairs by bimolecular capture of free charges on opposite sides of the polymer-polymer interface. If we assume that the capture process is dominated by lateral motion of charges close to the interface, then the rate of polaron pair formation is given by

$$F_X=\frac{n_{int}p_{int}h(\mu_{n0}+\mu_{p0})e}{3\varepsilon_0\varepsilon_r}, \tag{22}$$

where n_{int} is the electron density in the electron-transporting layer at the interface and p_{int} is the hole density in the hole-transporting layer at the interface. This expression is likely to underestimate the capture rate due to anisotropy in the carrier mobilities, however, we find that our results are relatively insensitive to the exact value of the capture rate.

We do not have direct measurements of the recombination rates or zero-field dissociation rates of polaron pairs in our system, and we must therefore examine the effects of a range of reasonable values for these parameters in our model. Polaron pair lifetimes have been measured to be in the range μs to ms at other organic-organic and organic-inorganic interfaces,[20–22] consistent with weak wave-function overlap between electron and hole, leading to nonradiative decay. Although this recombination mechanism is slow, it will nevertheless become important close to V_{oc}, where the majority of photogenerated polaron pairs must recombine, leading to significant polaron pair densities. We will see later that the ratio of polaron pair dissociation and recombination rates at a given internal field determines the efficiency of the device, which allows us to find reasonable values for the zero-field dissociation rate.

The boundary conditions for injection and extraction of charges at the electrodes require special attention for the case of photovoltaic devices. Below V_{oc}, electrons will flow towards the cathode and holes towards the anode, leading to a net extraction of carriers at the electrodes. Above V_{oc}, there will be a net injection of carriers at the electrodes. At V_{oc}, the injection and extraction currents will be exactly balanced. This condition occurs with a nonzero field at the electrodes, and we therefore need an injection mechanism which gives a zero net current at a finite field. To achieve this, we have used the model of Scott and Malliaras, which considers thermionic injection of carriers in the presence of Langevin-like recombination of injected carriers with their image charges.[15] However, we cannot use the final form of their result for the net current in the absence of photoinduced carriers, since this gives zero current at zero field. Instead, we use their intermediate result which considers injection and surface recombination separately

$$J=\frac{16\pi\varepsilon_r\varepsilon_0k_B^2N_0\mu T^2}{e^2}\exp(-\phi_B/k_BT)\exp f^{1/2}-n_0eS(E), \tag{23}$$

where the injection barrier is ϕ_B,

$$S(E)=\frac{4\pi\varepsilon_r\varepsilon_0(k_BT)^2\mu}{e^3}(1/\psi^2-f), \tag{24}$$

$$f=eEr_c/k_BT, \tag{25}$$

$$\psi(f)=f^{-1}+f^{-1/2}-f^{-1}(1+2f^{1/2})^{1/2}, \tag{26}$$

n_0 is the local carrier density close to the electrode, and E is the local electric field. Photogenerated carriers are included self-consistently through their contribution to n_0.

At negative fields, we treat the injection using a similar approach to the polaron pair dissociation rate discussed

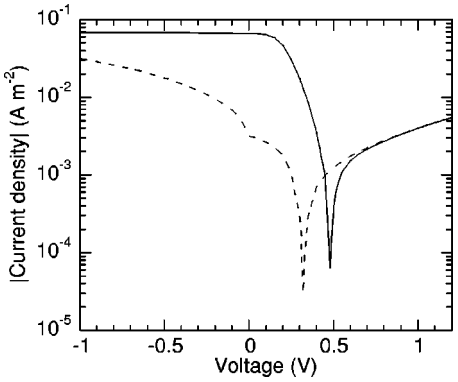

FIG. 4. Modeled current density versus internal voltage for an anode/PFB[50 nm]/F8BT[100 nm]/cathode device with a polaron pair generation rate of 4.3×10^{17} m^{-2} s^{-1} and $\tau_{diss}=10$ μs. Mobilities and injection conditions are described in the text. The polaron pair lifetime τ_{rec} is 1 ms (solid line), and 1 μs (dashed line).

above. The injection barrier is increased by an amount $e|E|r_c/4$, representing the additional energy required to move against the field to a distance at which the coulombic binding energy between the charge and its image is reduced to k_BT. The recombination velocity remains equal to its zero-field value, giving

$$J=\frac{16\pi\varepsilon_r\varepsilon_0 k_B^2 N_0 \mu T^2}{e^2}\exp[-(\phi_B-eEr_c/4)/k_BT] - n_0 eS(0). \quad (27)$$

The final parameters required in our model are the mobilities of carriers in the various materials. Here, we use an electron mobility in F8BT of $\mu_{n0}=3\times10^{-10}$ m^2 V^{-1} s^{-1}, $\gamma=1.55\times10^{-3}$ m$^{1/2}$ V$^{-1/2}$, and an hole mobility in PFB of $\mu_{p0}=1\times10^{-10}$ m^2 V^{-1} s^{-1}, $\gamma=3.00\times10^{-4}$ m$^{1/2}$ V$^{-1/2}$. These values are approximately two orders of magnitude lower than the values measured by time-of-flight techniques,[23,24] however, we have found that our values give a much better agreement to the current densities measured in single-layer LEDs.[25] The exact values of mobilities are not critical to the physics of our model; they simply determine the intensity at which space-charge effects become important.

IV. RESULTS AND DISCUSSION

Figure 4 (solid line) shows the calculated current-voltage characteristic for a device using the parameters described above, with a polaron pair generation rate of 4.3×10^{17} m^{-2} s^{-1}. In this simple example, we take $\tau_{rec}=1$ ms and $\tau_{diss}=10$ μs. The model reproduces many important features in the experimental curves, and there is an open-circuit voltage of 0.483 V. The operation of the device can be understood in more detail by studying the electric field, electron density, and hole density as a function of position within the device at various voltages, as shown in Figs. 5 and 6. We choose -0.5 V, corresponding to short-circuit conditions for a device with an aluminum cathode, 0 V,

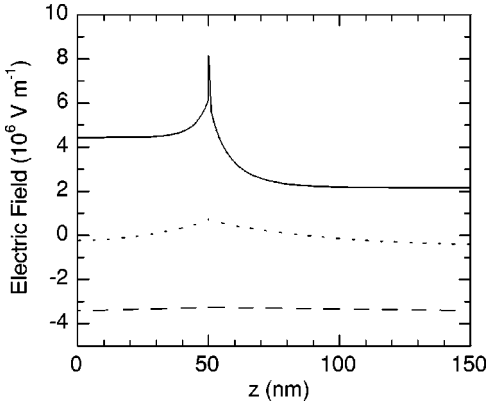

FIG. 5. Electric field versus position with $\tau_{rec}=1$ ms, at $V=0.483$ V (solid line), 0 V (dotted line), and -0.5 V (dashed line). The polaron pair generation rate is 4.3×10^{17} m^{-2} s^{-1}.

which would give flat bands in the absence of illumination, and 0.483 V, the open-circuit voltage. At -0.5 V, the variation of field through the device is small, indicating that space-charge effects are unimportant. There is sufficient negative field to give rapid separation of polaron pairs at the interface, so recombination is negligible and the quantum efficiency is close to 1. (For the purposes of modeling we define the quantum efficiency as the number of carriers flowing in the external circuit per exciton dissociation event. The measured quantum efficiencies will be lower since not all excitons reach the interface.) The current close to the interface is predominantly a drift current, with diffusion becoming important only near the electrodes where carrier densities are reduced. Close to the interface, the carrier densities are slowly varying; the difference in carrier density on either side of the interface is due to the difference in carrier mo-

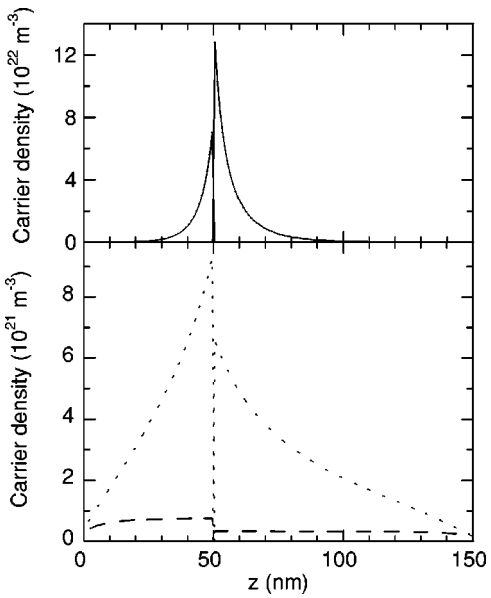

FIG. 6. Hole density ($z<50$ nm) and electron density ($z>50$ nm) versus position with $\tau_{rec}=1$ ms, at $V=0.483$ V (solid line), 0 V (dotted line), and -0.5 V (dashed line). The polaron pair generation rate is 4.3×10^{17} m^{-2} s^{-1}.

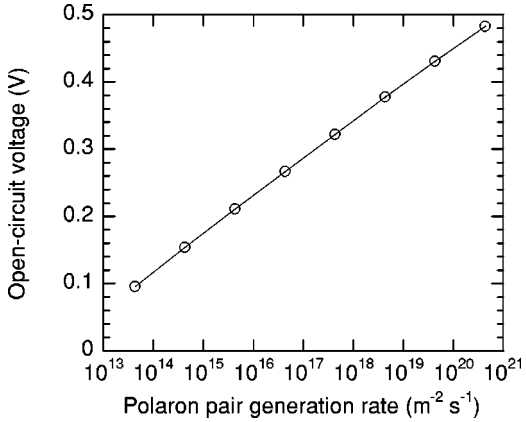

FIG. 7. Open-circuit voltage versus polaron pair generation rate with $\tau_{rec}=1$ μs.

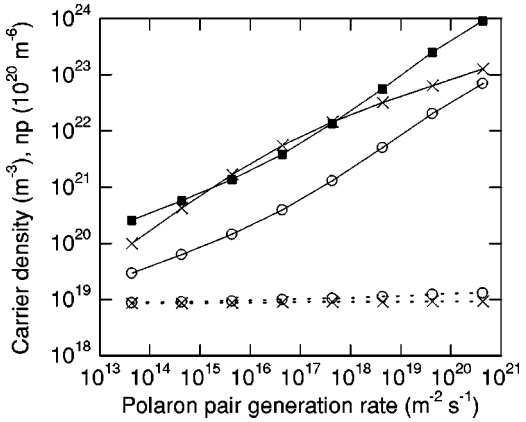

FIG. 8. Electron (crosses) and hole (circles) densities at the interface (solid lines) and the electrodes (dotted lines), as a function of polaron pair generation rate, at open circuit. The product of electron and hole densities at the interface is also shown (squares).

bilities in F8BT and PFB. At 0 V, the average field in the device is zero. Due to the low fields, the mobilities are low, and space-charge effects become more noticeable, causing the electric field to go slightly positive at the interface. Despite this reverse field, there is still sufficient polaron pair dissociation to give a quantum efficiency in excess of 0.97. In contrast to the -0.5 V case, the current is predominantly due to diffusion, driven by the carrier concentration gradient away from the interface. In other words, the device still operates as a photovoltaic device despite the absence of a net internal field. To achieve a total current of zero requires an additional positive voltage to produce a drift current to cancel out the diffusion. Under these open-circuit conditions a polaron pair density of 4.3×10^{14} m^{-2} builds up at the interface, leading to a polaron pair recombination rate equal to the generation rate of 4.3×10^{17} $m^{-2}\,s^{-1}$. There is rapid dissociation of polaron pairs into free charges, balanced by an identical rate of bimolecular recombination (5.5×10^{18} $m^{-2}\,s^{-1}$). To achieve this high bimolecular recombination rate requires large carrier densities at the interface and hence throughout the device. The high carrier densities lead to a significant change of electric field within the device. The carrier densities decay rapidly away from the interface in order to maintain a balance between drift and diffusion current throughout the device.

The example above chose a polaron pair recombination time that was long compared with typical dissociation times, leading to high quantum efficiencies at voltages as little as 0.3 V below the open-circuit voltage. However, the experimental data show that the quantum efficiency rises with negative voltage up to at least 1 V below the open-circuit voltage. This indicates that polaron pair recombination must compete with dissociation over this range of fields. To reproduce this behavior, we have tried reducing τ_{rec} from 1 ms to 1 μs, whilst maintaining the same value of $\tau_{diss}=10$ μs. The current-voltage curve (Fig. 4, dashed line) shows a linear increase in photocurrent with increasing negative voltage, with the quantum efficiency increasing from 0.05 at 0 V to 0.46 at -1 V.

The modeled intensity dependence of V_{oc} is shown in Fig. 7. The experimentally observed logarithmic dependence of V_{oc} on intensity is reproduced over a wide range of intensities. The model shows an increase in V_{oc} with intensity of 55 mV per decade, slightly lower than the value of 60 mV per decade predicted by the simple analytical model of Eq. (4) taking $\alpha=0.5$ and assuming a constant carrier density at the electrodes. To investigate the origin of this discrepancy, it is useful to examine the intensity dependence of the carrier densities in the device at open circuit, as shown in Fig. 8. The polaron pair density at the interface is proportional to the intensity, as expected for monomolecular recombination. The densities of free electrons and holes at the interface are not equal, and increase sublinearly with intensity, although not exactly as $I^{0.5}$. This complex behavior is a consequence of the asymmetry in layer thicknesses and mobilities. However, the product of electron and hole densities at the interface is only weakly dependent on intensity, consistent with a bimolecular recombination process. The electron and hole densities at the interface are determined as follows. At open circuit, the polaron pair dissociation rate must be equal to the generation rate; this sets the polaron pair density. Since there is no net flow of free charges away from the interface, the rates of polaron pair dissociation to free charges and formation from free charges must be equal. The dissociation rate is determined by the polaron pair density and the local electric field, but the rate constant is only weakly dependent on field at positive fields, and the field at open circuit varies only slowly with the intensity. The dissociation and formation rates are, therefore, approximately proportional to intensity. The formation rate is also given by Eq. (22), and is proportional to the product of the free electron and hole densities at the interface. The product of free electron and hole densities is, therefore, approximately proportional to intensity, which would in a symmetrical device give free-carrier densities proportional to $I^{0.5}$. So, although the final loss mechanism is monomolecular decay of polaron pairs, the process which controls the free charge densities, and hence the open-circuit voltage, is a bimolecular process leading to $\alpha\approx0.5$.

Figure 8 also shows that the carrier densities at the electrodes increase slightly with the incident intensity, although by less than 50% over the 7 orders of magnitude of intensity studied. This will also contribute to the lowering of the in-

tensity dependence of the V_{oc} in the numerical model compared with the simple analytical model, although this contribution is less important than the field dependence of the polaron pair dissociation rate discussed above.

It is interesting to examine the effect of space charge on V_{oc}. In the numerical model, the ratios of carrier densities at the interface and the electrode are found to obey Eq. (1) accurately, even when space charge causes a significant change in field within the device. This is as expected on thermodynamic grounds, where only the total potential difference influences the population ratio, independent of the intervening potential landscape. Space charge, therefore, only plays a minor role at open circuit, through its influence on the local electric field at the interface and on the split of the total potential between the two layers.

Comparing now with the experimental data, both the analytical model and the numerical model underestimate the observed intensity dependence of the open-circuit voltage of 0.8 V per decade. They also do not reproduce the saturation behavior which is observed. The stronger intensity dependence in the experiment implies that $\alpha > 0.5$, indicating a more linear dependence of the free charge density on intensity. This might be due to the involvement of a fixed density of ''trap'' sites in the process of polaron formation from free charges. This will be the subject of future investigation. The saturation of V_{oc} at high intensities implies a saturation of the polaron pair density at the interface. This might arise due to high densities of free charges or polaron pairs at the interface leading to nonradiative quenching of photogenerated excitons before charge separation can occur. With an exciton diffusion range of 5 nm, for example, one would expect very strong quenching at charge densities of 8×10^{24} m^{-3}. Another possibility is that a high density of polaron pairs at the interface might cause a sufficient field at the interface [Eqs. (12) and (13)] to make it energetically unfavorable to dissociate further excitons. This mechanism would be particularly effective in the PFB/F8BT system, where the band offset is believed to be only just sufficient for charge transfer to occur. At a given polaron pair generation rate, the voltage drop due to polaron pairs at the interface depends strongly on the polaron pair lifetime. For $\tau_{rec}=1$ μs, the voltage drop is less than 2 mV at a polaron pair generation rate of 4.3×10^{20} m^{-2} s^{-1}, but with $\tau_{rec}=1$ ms, the voltage can reach significant values in excess of 100 mV at polaron pair generation rates above 2×10^{19} m^{-2} s^{-1}. Where band offset at the interface is more than large enough to drive charge separation, some of the incident energy will be wasted as heat. In this case, a localized field at the interface can reduce the energy wasted by raising the energy of the charge-separated state. The carriers are then collected at a higher potential, such that the potential dropped at the interface contributes directly to the open-circuit voltage. As explained above, the open-circuit voltage will saturate when there is no longer a driving force for charge separation. This mechanism might explain the reported dependence in some systems of the measured open-circuit voltage on the band offset between the electron- and hole-accepting material.[6]

Next, we examine the device characteristics away from open-circuit conditions. We have already seen that at negative voltages, the current close to the interface becomes dominated by drift rather than diffusion, and that the quantum efficiency depends on the competition between polaron pair recombination and dissociation. Figure 9 shows how the quantum efficiency varies with intensity at an internal voltage of -0.5 V (corresponding to short-circuit conditions in a device with an Al cathode) with $\tau_{rec}=1$ μs and $\tau_{diss}=10$ μs. The quantum efficiency remains constant as seen experimentally, until very high intensities where it begins to reduce. This behavior can be understood by examining the charge and field distributions in the device at polaron pair generation rates of 4.3×10^{15} m^{-2} s^{-1} and 4.3×10^{19} m^{-2} s^{-1} (Figs. 10 and 11). At low intensity the electric field is constant and drift dominates at the interface. At high intensities, however, space charge in the device significantly reduces the electric field at the interface (i.e., the field becomes less negative), leading to reduced polaron pair dissociation and lower efficiencies. Since the electric field at the interface is reduced, drift of carriers away from the interface is suppressed and diffusion begins to play a larger role in the current. This behavior is analogous to the space-charge-limited current flow commonly observed in polymer LEDs, where injection is suppressed by reducing the field at the electrode, but in the photovoltaic case it is the field at the central interface which is reduced in order to suppress charge

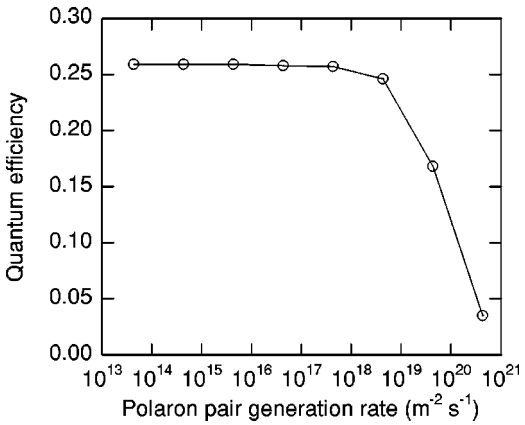

FIG. 9. Quantum efficiency versus polaron pair generation rate at -0.5 V with $\tau_{rec}=1$ μs.

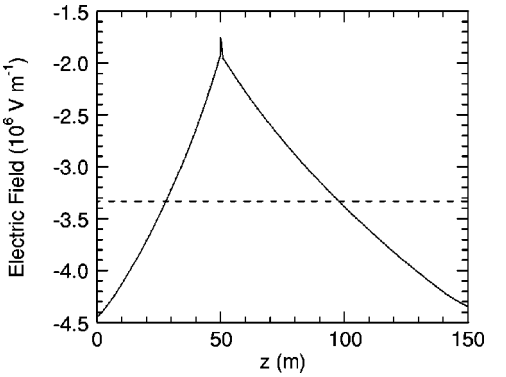

FIG. 10. Electric field versus position at -0.5 V with $\tau_{rec}=1$ μs at polaron pair generation rates of 4.3×10^{15} m^{-2} s^{-1} (dashed line) and 4.3×10^{19} m^{-2} s^{-1} (solid line).

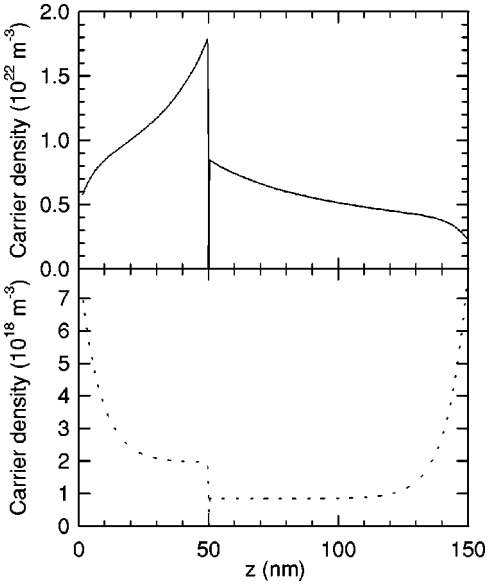

FIG. 11. Hole ($z<50$ nm) and electron ($z>50$ nm) densities versus position at -0.5 V with $\tau_{rec}=1$ μs at polaron pair generation rates of 4.3×10^{15} m^{-2} s^{-1} (dashed line) and 4.3×10^{19} m^{-2} s^{-1} (solid line).

generation there. It should be noted that in photovoltaic devices these effects do not become important until very high intensities.

Finally, we examine the effect of the injection process at the electrodes on the current-voltage characteristics. Figure 12 shows the current-voltage characteristics for devices with cathode barriers, ϕ_B, of 0.4, 0.5, and 0.6 eV, and anode barriers of 0.5 eV. As expected, the major difference in the characteristics is in the magnitude of the current above V_{oc}, which is associated with carrier injection. There is also an effect on the size of V_{oc}, which takes values of 0.224 V, 0.322 V, and 0.419 V with barriers of 0.4 eV, 0.5 eV, and 0.6 eV, respectively. According to Eq. (4), the major effect of the injection barrier is through the carrier density at the contact,

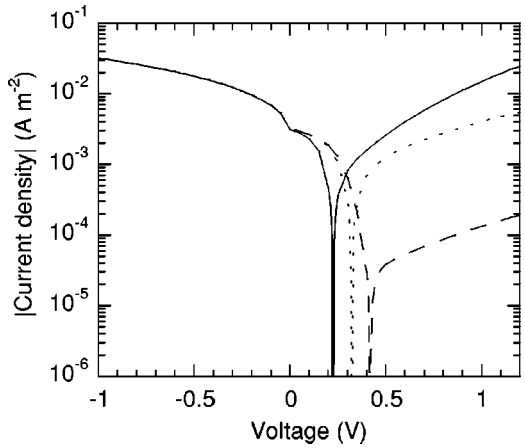

FIG. 12. Modeled current-voltage curves with $\tau_{rec}=1$ μs and a polaron pair generation rate of 4.3×10^{17} m^{-2} s^{-2}. The anode barrier is 0.5 eV and the cathode barrier is 0.4 eV (solid line), 0.5 eV (dotted line), or 0.6 eV (dashed line).

which takes values of 4.13×10^{20} m^{-3}, 9.29×10^{18} m^{-3}, and 2.02×10^{17} m^{-3} with increasing ϕ_B. If the carrier density at the contact maintained itself close to thermal equilibrium $n_0=N_0\exp(-\phi_B/k_BT)$, then according to Eq. (4) reducing the injection barrier would cause an identical reduction in V_{oc}. In our model, the carrier densities are not far from the equilibrium values, so V_{oc} does indeed reduce with cathode barrier height. This predicts that the measured open-circuit voltage (the sum of the internal V_{oc} and the difference in electrode work functions) would be insensitive to the cathode work function. This is in contradiction to our experimental results, which show that the measured open-circuit voltage increases with the electrode work function difference, leading to a constant internal V_{oc}. We note, however, that the model of Scott and Malliaras[15] completely neglects the effects of disorder, which may have a major effect on the detailed injection rates and carrier densities.[26] More work is, therefore, necessary in order to predict the absolute value of the open-circuit voltage in any given device structure, however, this does not affect the intensity dependence which is related to processes at the polymer-polymer interface rather than at the electrodes.

V. CONCLUSIONS

We have developed a numerical model for the current-voltage characteristics of bilayer polymer photovoltaic devices. The model includes drift and diffusion currents, injection and extraction at the electrodes, and the effects of space charge on the electric field within the device. In order to explain the linear dependence of photocurrent on intensity, even when recombination at the interface limits the device efficiency, we consider that generation of free charges takes place via dissociation of an intermediate population of bound polaron pairs at the interface. We develop expressions for the formation and dissociation of polaron pairs as a function of applied field. Our model reproduces many of the important features of the measured current-voltage characteristics of polyfluorene-based bilayer photovoltaic devices, including the logarithmic dependence of open-circuit voltage on intensity. The model will allow optimization of device performance by investigating the effects of material parameters on device characteristics, and we can already identify a number of design rules to achieve efficient photovoltaic operation. Short-circuit quantum efficiency is determined by the competition between polaron pair dissociation and recombination at the field determined by the difference in electrode work functions. Increasing the dissociation rate (for example by reducing the polaron pair binding energy) will increase the efficiency. Decreasing the recombination rate will have a similar effect, although this may lead to a saturation of the polaron pair density at high intensities. The measured open-circuit voltage will depend not only on the difference in electrode work functions, but also on the intensity and the charge densities at the electrodes. Reducing the charge densities at the electrodes will increase the open-circuit voltage; this may be achieved by suppressing charge carrier injection, for example by increasing the injection barrier or reducing the density of chargeable sites in the polymer. Finally, the fill factor

is determined by the shape of the current-voltage curve between short-circuit and open-circuit conditions. It is optimized when polaron pair dissociation competes effectively with recombination even with a small field in the positive direction. Under these conditions the quantum efficiency rises rapidly to unity at voltages only slightly below the open-circuit voltage, leading to a rectangular current-voltage curve with a large fill factor.

ACKNOWLEDGMENTS

This work was supported by the Engineering and Physical Sciences Research Council, UK.

[1] J.J.M. Halls and R.H. Friend, in *Clean Energy from Photovoltaics*, edited by M.D. Archer and R. Hill (Imperial College Press, London, 2001), Chap. 9, pp. 377–445.
[2] S.E. Shaheen, C.J. Brabeck, N.S. Sariciftci, F. Padinger, T. Fromherz, and J.C. Hummelen, Appl. Phys. Lett. **78**, 841 (2001).
[3] J.J.M. Halls, C.A. Walsh, N.C. Greenham, E.A. Marseglia, R.H. Friend, S.C. Moratti, and A.B. Holmes, Nature (London) **376**, 498 (1995).
[4] M. Granström, K. Petritsch, A.C. Arias, A. Lux, M.R. Andersson, and R.H. Friend, Nature (London) **395**, 257 (1998).
[5] R. H. Bube, *Photoelectronic Properties of Semiconductors* (Cambridge University Press, Cambridge, 1992).
[6] C.J. Brabec, A. Cravino, D. Meissner, N.S. Sariciftci, T. Fromherz, M.T. Rispens, L. Sanchez, and J.C. Hummelen, Adv. Funct. Mater. **11**, 374 (2001).
[7] J. Liu, Y. Shi, and Y. Yang, Adv. Funct. Mater. **11**, 420 (2001).
[8] G.G. Malliaras, J.R. Salem, P.J. Brock, and J.C. Scott, J. Appl. Phys. **84**, 1583 (1998).
[9] C.M. Ramsdale, J.A. Barker, A.C. Arias, J.D. MacKenzie, R.H. Friend, and N.C. Greenham, J. Appl. Phys. **92**, 4266 (2002).
[10] B.K. Crone, I.H. Campbell, P.S. Davids, D.L. Smith, C.J. Neef, and J.P. Ferraris, J. Appl. Phys. **86**, 5767 (1999).
[11] G.G. Malliaras and J.C. Scott, J. Appl. Phys. **85**, 7426 (1999).
[12] P.W.M. Blom, M.J.M. de Jong, and S. Breedijk, Appl. Phys. Lett. **71**, 930 (1997).
[13] D.J. Pinner, R.H. Friend, and N. Tessler, J. Appl. Phys. **86**, 5116 (1999).
[14] Y. Roichman and N. Tessler, Appl. Phys. Lett. **80**, 1948 (2002).
[15] J.C. Scott and G.G. Malliaras, Chem. Phys. Lett. **299**, 115 (1999).
[16] L.A.A. Pettersson, L.S. Roman, and O. Inganäs, J. Appl. Phys. **86**, 487 (1999).
[17] R. Bilke, A. Schreiber, I. Bleyl, D. Haarer, and D. Adam, J. Appl. Phys. **87**, 3872 (2000).
[18] U. Albrecht and H. Bässler, Chem. Phys. Lett. **235**, 389 (1995).
[19] A.K. Jonscher, Thin Solid Films **1**, 213 (1967).
[20] D.S. Ginger and N.C. Greenham, Phys. Rev. B **59**, 10 622 (1999).
[21] L. Smilowitz, N.S. Sariciftci, R. Wu, C. Gettinger, A.J. Heeger, and F. Wudl, Phys. Rev. B **47**, 13 835 (1993).
[22] D.M. Russell, A.C. Arias, R.H. Friend, C. Silva, C. Ego, A.C. Grimsdale, and K. Müllen, Appl. Phys. Lett. **80**, 2204 (2001).
[23] M. Redecker, D.D.C. Bradley, M. Inbasekaran, W.W. Wu, and E.P. Woo, Adv. Mater. **11**, 241 (1999).
[24] A.J. Campbell, D.D.C. Bradley, and H. Antoniadis, Appl. Phys. Lett. **79**, 2133 (2001).
[25] A.S. Dhoot, Ph.D. thesis, University of Cambridge, 2001.
[26] U. Wolf, V.I. Arkhipov, and H. Bässler, Phys. Rev. B **59**, 7507 (1999).